Dalton Transactions

PAPER

View Article Online
View Journal | View Issue

Cite this: *Dalton Trans.*, 2015, **44**, 10852

Valence properties of Cu and Ru in titanium-substituted $LnCu_3Ru_4O_{12+\delta}$ (Ln = La, Pr, Nd) investigated by XANES and TGA†

Stefan Riegg,*[a] Armin Reller,[b] Alois Loidl[a] and Stefan G. Ebbinghaus[c]

Received 17th December 2014,
Accepted 17th March 2015

DOI: 10.1039/c4dt03876b

www.rsc.org/dalton

In the solid-solution series $La_yCu_3Ru_xTi_{4-x}O_{12+\delta}$ ($0 \le x \le 4$) the Cu and Ru electronic states are highly correlated. With increasing Ru content x the system properties change from a paramagnetic insulator with colossal dielectric constant to a heavy-fermion metal. To further elucidate the occurring phase transitions, the valences of Cu and Ru have been investigated utilizing XANES measurements at the Cu-K and the Ru-K absorption edges. It was found that the Ru oxidation number is close to +4 in all samples, while the Cu valence linearly decreases from +2 for the titanate (x = 0) to +1.6 for the ruthenate (x = 4). Additional thermogravimetric measurements have been used to determine the oxygen content and rather high oxygen excesses up to $\delta \approx 0.7$ (for x = 0.5) were obtained. The additional oxygen for $x < 2$ is required to compensate the constant Ru +4 valence. Our findings are in accordance with the reported phase transitions of the magnetic and transport properties. Both the valence shift and the shapes of the absorption edges suggest a change from localized to itinerant character of the Cu electronic states with increasing x, while the Ru electrons remain localized. Analogous results concerning the valences were found for the $Pr_yCu_3Ru_xTi_{4-x}O_{12+\delta}$ and $Nd_yCu_3Ru_xTi_{4-x}O_{12+\delta}$ solid-solution series.

1 Introduction

Perovskites with sum formula ABO_3 are one prototypical subject for studies of structure–property relationships in transition-metal oxides. This is due to the fact that a plethora of different compositions can easily be obtained. By this the physical properties can be tailored *via* the electronic configuration of A- and/or B-type cation as well as *via* changes in bond lengths and bond angles, which are the result of the size mismatch of A- and B-site cations.

The family of cubic $AA'_3B_4O_{12}$ compounds (Space group $Im\bar{3}$, no. 204) can be derived from the perovskite structure by a collective rotation of the BO_6 octahedra around <111> (according to a threefold tilting $a^+a^+a^+$ in Glazer's notation).[1,2] This rotation leads to a strong deformation of 3/4 of the A-sites resulting in a square-planar coordination for the cations occupying this site, which is therefore denoted as A′. This coordination geometry is favored by Jahn–Teller active ions like Cu^{2+} and Mn^{3+}.[3] The crystal structure of the $AA'_3B_4O_{12}$ perovskites is depicted in Fig. 1.

The solid-solution series $La_yCu_3Ru_xTi_{4-x}O_{12}$ is a member of this $AA'_3B_4O_{12}$ family and exhibits a rich phase diagram of physical properties depending on the B-site composition x.[4–6] The pure titanate (x = 0) is insulating with a colossal dielectric constant similar to $CaCu_3Ti_4O_{12}$.[7–9] Below $T_N \approx 25$ K an antiferromagnetic long-range order of the localized Cu^{2+} (S = 1/2) spin moments occurs. Until x = 0.5 the Néel temperature decreases linearly and a spin-glass state was identified by ac-susceptibility measurements for $0.5 < x < 2.5$.[10] On the other hand, for $x \ge 2.5$ the ruthenium-rich phases are metallic and due to electronic correlation effects exhibit heavy-fermion behavior.[5] This behavior is usually observed in materials containing 4f or 5f elements due to hybridization of localized f-electrons and typically s- or p-derived conduction electrons. Very rarely, transition-metal oxides without f-elements can also exhibit heavy-fermion properties due to strong correlation effects of localized and itinerant d-electrons. Examples of such d derived heavy-fermion materials are LiV_2O_4 and $CaCu_3Ru_4O_{12}$.[11–15] $CaCu_3Ru_4O_{12}$ in addition provides non-Fermi liquid behavior below 2 K as well as an intermediate-valence behavior caused by d electron fluctuations.[16] This compound is closely related to the $Ln_yCu_3Ru_xTi_{4-x}O_{12}$ series investigated in this work.

[a]*Experimental Physics V, Center for Electronic Correlations and Magnetism, University of Augsburg, D-86159 Augsburg, Germany. E-mail: stefan.riegg@physik.uni-augsburg.de; Fax: +49 821 598 3649; Tel: +49 821 598 3751*

[b]*Resource Strategy, University of Augsburg, D-86159 Augsburg, Germany*

[c]*Solid State Chemistry, Martin Luther University Halle-Wittenberg, D-06099 Halle, Germany. E-mail: stefan.ebbinghaus@chemie.uni-halle.de*

†Electronic supplementary information (ESI) available. See DOI: 10.1039/c4dt03876b

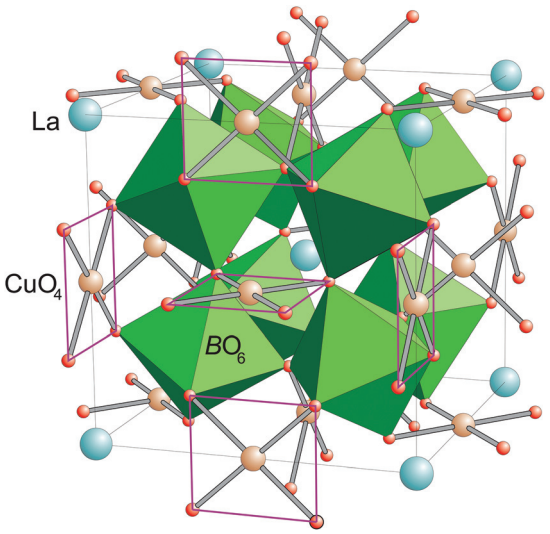

Fig. 1 (color online) Crystal structure of $La_yCu_3Ru_xTi_{4-x}O_{12}$. La ions are shown as large turquoise spheres, while Cu is colored brown and oxygen is represented by small red spheres. The $(Ru/Ti)O_6$ octahedra are colored green. In the CuO_4 plaquettes grey Cu–O bonds and additional red lines emphasize the square-planar coordination.

The transition from the Mott-insulating spin-glass state to the heavy-fermion metal in $La_yCu_3Ru_xTi_{4-x}O_{12}$ was observed at approximately $x = 2.25$ and ascribed to a quantum-critical point at this composition.[5,17,18] The appearance of various phase transitions within a rather small substitution range is highly attractive for more detailed investigations. The complete solid-solution series was therefore synthesized with La, Pr, and Nd occupying the A-site according to the sum formula $Ln_yCu_3Ru_xTi_{4-x}O_{12}$. Up to now, the discussion of Kondo-like behavior in the ruthenium rich phases based on magnetic susceptibility, specific heat, resistivity, and magnetic resonance experiments was performed without valence analysis of Ru or Cu. A detailed study of the oxygen content in these materials has not been carried out either. There already have been considerations about the changing valence state of copper in $La_yCu_3Ru_xTi_{4-x}O_{12}$ in ref. 4. However, distinct charge-transfer properties similar to $CaCu_3Ru_4O_{12}$ were neither observed in the magnetic susceptibility nor in temperature-dependent crystal-structure data of $LnCu_3Ru_4O_{12}$.[5,6]

It is apparent that physical properties such as electrical conductivity and magnetism react very sensitively on the oxygen content as well as on the cationic valences. By variation of the oxygen content, the concentration of free charge carriers can be controlled and a direct influence on the transport properties of the material is possible. To better understand the above described variations of the investigated magnetic properties and the metal-to-insulator transition in $La_yCu_3Ru_xTi_{4-x}O_{12}$, valences and oxygen stoichiometry have to be determined. The accurate description of Ru and Cu valence was performed using X-ray absorption near edge structure (XANES) studies. In addition, the oxygen content for the La series was obtained from thermogravimetric (TG) measurements under reducing atmosphere. A possible deviation from the nominal oxygen stoichiometry is denoted as δ in the sum formula $La_yCu_3Ru_xTi_{4-x}O_{12+\delta}$.

2 Experimental

Polycrystalline samples of $Ln_yCu_3Ru_xTi_{4-x}O_{12+\delta}$ were synthesized by a conventional solid-state reaction using binary oxides as starting products. La_2O_3 (Chempur, 99.9%), Pr_2O_3 (MaTecK, 99.9%), Nd_2O_3 (Chempur, 99.9%), and RuO_2 (Chempur, 99.9%) were dried at 900 °C for 6 hours to remove water and carbonates. During this pre-drying step Pr_2O_3 reacted to form the non-hygroscopic Pr_6O_{11}. Appropriate amounts of these oxides were mixed with TiO_2 (Aldrich, ≥99%) and CuO (HelmAG, 99.5%) to achieve 2 g of the final product. An excess of CuO of roughly 0.3 g per g sample is used as self-flux and was dissolved after the reaction with diluted hydrochloric acid.[19] The mixed powders were ground using agate mortar and pestle and pelletized to avoid reaction with the crucible material (highly densified aluminium oxide). The pellets were heated in air at 1040 °C for 96 hours with one intermediate grinding and pelletizing step after 48 hours. Phase purity was checked by X-ray diffraction. Details of the excellent purity of the $La_yCu_3Ru_xTi_{4-x}O_{12+\delta}$ samples have already been reported in ref. 18. The samples of the other two series $Pr_yCu_3Ru_xTi_{4-x}O_{12+\delta}$ and $Nd_yCu_3Ru_xTi_{4-x}O_{12+\delta}$ are of equivalent quality (see Fig. 1, 2 in the ESI†).

X-ray diffraction patterns of the powder samples were recorded at room temperature in the angular range $10° \leq 2\theta \leq 150°$ using a Seifert 3003 TT θ–θ powder diffractometer ($Cu\text{-}K_{\alpha1,2}$ radiation) equipped with a one-dimensional single-line semiconductor detector (METEOR-1D). A step width of 0.01° 2θ and an integration time of 300 s per data point were chosen. The Rietveld structure analysis was carried out with the FullProf program suite.[20]

For the thermogravimetric (TG) measurements a TA-Instruments Q500 thermobalance was used. Approximately 30 mg of sample powders were heated in platinum crucibles at a constant rate of 10 K min^{-1} from room temperature to 950 °C under forming gas flow of 75 ml min^{-1} (5% H_2 in N_2) and held at this maximum temperature for 15 min. For buoyancy correction a baseline was recorded using roughly 40 mg of dry Al_2O_3 and subtracted from the sample measurements.

XANES investigations at the Cu-K (8.979 keV) and the Ru-K (22.117 keV) absorption edges were carried out in the transmission mode at the beamline X at HASYLAB (DESY, Hamburg).[21] For the measurement appropriate amounts of sample or reference material were mixed with 20 mg cellulose and pressed into pellets of 13 mm diameter. For measurements at the Cu-K edge approximately 10 mg of the binary oxides were used, while for the $ACu_3B_4O_{12}$ samples with significantly lower Cu content only 30 mg could be taken to keep the absorption within a reasonable range. For the Ru-K edge measurements (at significantly higher energies) the sample weight varied between 60 mg and 120 mg according to

0.25 mmol ruthenium. The absorption spectra of CuO and Cu_2O were recorded as references for Cu^{2+} and Cu^{1+}, respectively. Additional Cu^{2+} references (isostructural to the investigated samples) were $CaCu_3Ti_4O_{12}$ and $SrCu_3Ti_4O_{12}$. Different ruthenates were used as Ru^{4+} and Ru^{5+} references,[6,22] while Ru-acetylacetonate and Ru-nitrosylacetonate served as trivalent ruthenium references. All spectra were energy calibrated using a Cu metal foil or Ru metal powder as simultaneously measured references. The pre-edge region was used for a linear fit, which was subtracted from the spectra over the whole energy range. These background-corrected spectra were normalized with respect to a common region above the edge energy.

3 Crystal structure and oxygen stoichiometry

All samples crystallize in the space group $Im\bar{3}$ with statistically distributed Ti and Ru on the B-site (Wyckoff position 8*c*: $\frac{1}{4}\frac{1}{4}\frac{1}{4}$). The A′- (6*b*: $0\frac{1}{2}\frac{1}{2}$) and the O-sites (24 g: *xy*0, $x \approx 0.18$, $y \approx 0.31$) are fully occupied with Cu and oxygen, respectively. On the other hand, the A-site (2*a*: 000) shows only a 2/3rd occupation for the pure titanates due to the charge balance. With increasing ruthenium concentration this site becomes increasingly filled, which is expressed by the parameter y in $Ln_yCu_3Ru_xTi_{4-x}O_{12+\delta}$. The relation $y = 2/3 + x$ holds for $x \leq 0.33$, while for $x \geq 0.33$ the A-site is fully occupied and, hence, $y = 1$.

Both the increasing filling of the A-site and the slightly larger ionic radius of Ru^{4+} compared to Ti^{4+} have a strong impact on the evolution of the cell parameter *a* as shown in Fig. 2. A steep increase is observed for $x \leq 0.33$ dominated by the increasing A-site filling. In contrast, a much smaller slope is found for $x \geq 0.33$ reflecting the increasing ruthenium substitution level (ionic radii with coordination number (CN) 6: Ru^{4+}: 0.620 Å; Ti^{4+}: 0.605 Å).[23] For the Pr- and Nd-series systematically smaller values for *a* were obtained in agreement with smaller ionic radii for the Pr^{3+} and Nd^{3+} ions (ionic radii with CN 12: La^{3+}: 1.36 Å; Nd^{3+}: 1.27 Å; Pr^{3+}: 1.179 Å for CN 9 and scaled to CN 12 with factor 1.1 obtained from intrapolation of the corresponding values for La and Nd, resulting in 1.30 Å),[23] which is indicated by parallel solid lines in Fig. 2. The cell-parameter values for the Nd series are in very good agreement with data reported by Muller *et al.* in ref. 24. Details of the structural data such as refinement parameters, bond lengths and angles as well as the measured XRD patterns are given in the ESI.†

The oxygen stoichiometry of $La_yCu_3Ru_xTi_{4-x}O_{12+\delta}$ was obtained by TG measurements under reducing conditions. The late (noble) transition-metal cations of Cu and Ru are completely reduced to the respective metals leading to comparatively large weight losses between roughly 7% and 18% (see Fig. 3b). In contrast, La^{3+} and Ti^{4+} are stable up to the maximum temperature of 950 °C. Control experiments in synthetic air led to insignificant weight losses (<1.5‰), proving

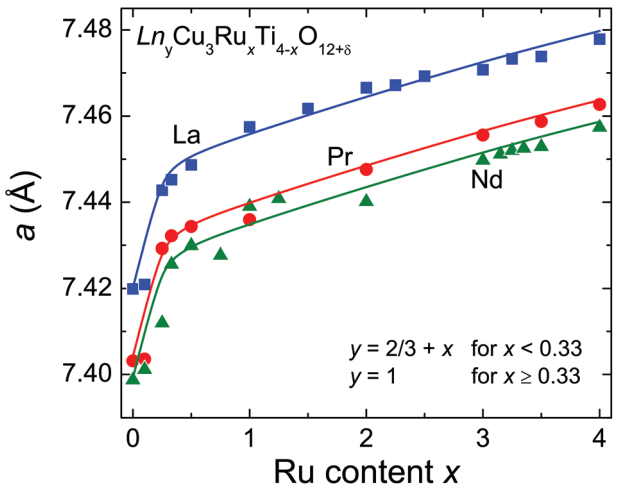

Fig. 2 (color online) Cell parameter *a* of the cubic unit cell for $Ln_yCu_3Ru_xTi_{4-x}O_{12+\delta}$ (Ln = La, Pr, Nd). The solid lines (drawn to guide the eye) shift by a constant value reflecting the different ionic radii of the Ln^{3+} ions.

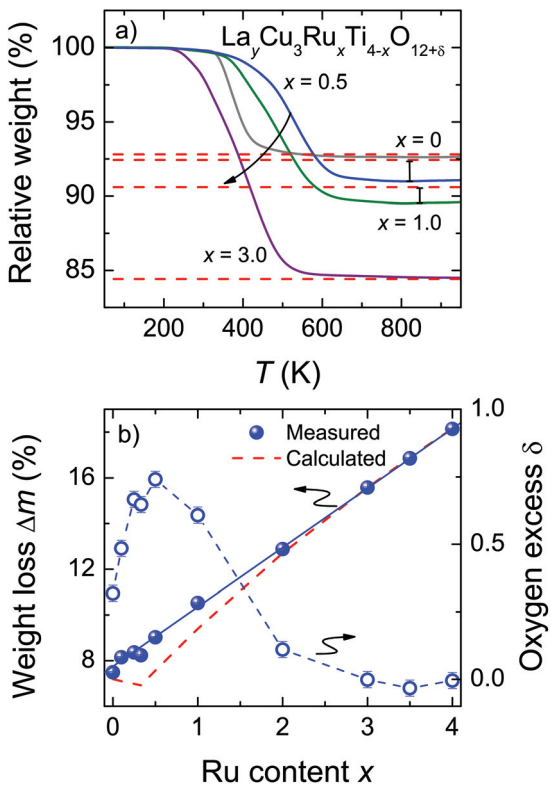

Fig. 3 (color online) (a) Relative sample weight from thermogravimetric measurements of $La_yCu_3Ru_xTi_{4-x}O_{12+\delta}$ for x = 0, 0.5, 1.0, 3.0. The horizontal dashed lines mark the expected weight after reduction according to the red dashed line in (b). The arrow indicates the shift of the inflection point. (b) Left scale: obtained relative weight losses (blue spheres) and expected values assuming Ru^{4+} and Cu^{2+} valences and $\delta = 0$ (dashed red line). Right scale: oxygen excess δ obtained from the difference between measured and expected weight losses (open blue circles).

that the samples do not contain any carbonates or hydroxides. Thus, after the TG measurements La_2O_3, TiO_2, Cu, and Ru are obtained as confirmed by powder XRD measurements.

The observed weight losses during the TG measurement occur at different temperatures depending on x (Fig. 3a). Above roughly 700 °C the reaction is completed for all samples as evidenced by the constant weight values up to the maximum temperature. For $La_{2/3}Cu_3Ti_4O_{12}$ a sudden weight decrease is observed at roughly 375 °C and the reaction is completed already at approximately 600 °C. Upon Ru substitution the reduction step becomes much broader and for $x \leq 0.5$ its inflection point is shifted to higher temperatures by roughly 150 °C. By further increasing the Ru content the weight reduction increases correspondingly and the temperature of the reduction step is monotonously shifted to lower temperatures (300 °C). This behavior reflects a decreasing shielding effect as reported for *e.g.* $SrTi_{1-x}Ru_xO_3$ and $Sr_2Ti_{1-x}Ru_xO_4$.[25] Under the chosen conditions no clearly separated reaction steps were observed, indicating an almost simultaneous reduction of Cu and Ru.

The obtained weight-loss values are depicted as blue spheres in Fig. 3b as a function of the ruthenium content. The reproducibility of approximately 10 μg for the measurements and the baseline correction correspond to an error of less than ±0.06%. The experimental data are increasing linearly with x as marked by a blue solid line resulting from a linear fit. The value for Δm was determined as the difference between 50 °C and 900 °C. For comparison, the theoretical weight loss was calculated presuming $\delta = 0$ according to the following equation:

$$La_yCu_3Ru_xTi_{4-x}O_{12} \xrightarrow{\Delta,H_2} y/2La_2O_3 + (4-x)TiO_2 + 3Cu + xRu + (4 + 2x - 1.5y)H_2O(\uparrow) \quad (1)$$

The fraction of volatile oxygen thus amounts to $z = 4 + 2x - 1.5y$. Using the molar masses of oxygen M(O) and of the samples before reduction M_i the expected weight losses Δm_{calc} can be calculated according to:

$$\Delta m_{calc} = z\frac{M(O)}{M_i}. \quad (2)$$

These values are drawn as a red dashed line in Fig. 3b. The deviation between the experimental and the calculated data reveals the presence of excess oxygen for low Ru substitution levels. In addition, the strongly varying shape of the two curves is noteworthy, because the kink in the calculated curve caused by the changing occupation of the Ln-site for $x \leq 0.33$ does not appear for the measured weight-loss values. From the experimental weight losses oxygen excesses up to $\delta = 0.74$ per f.u. were obtained for $x = 0.5$ (Fig. 3b, right scales). The value of δ is calculated according to:

$$\delta = \left(\frac{1}{1-\Delta m_{meas}} - 1\right)\frac{M_f}{M(O)} - z, \quad (3)$$

where Δm_{meas} is the measured weight loss and M_f is the molar mass of the non-volatile final reaction products. The occurrence of high oxygen excesses in $ACu_3B_4O_{12}$-type perovskites has already been observed for the system $Cu_{2-x}Ta_4O_{12+\delta}$ where δ reaches values up to 0.45.[26]

4 Cation valence determination using X-ray absorption spectroscopy

The Ru and Cu valences were determined using XANES spectroscopy. Assuming a constant 2+ oxidation state for the Cu ions and $\delta = 0$, a Ru valence of nominal +3.75 would result for $LnCu_3Ru_4O_{12}$. In fact, a constant Ru valence close to +4 was reported for $LaCu_3Ru_xTi_{4-x}O_{12}$ and $NdCu_3Ru_xTi_{4-x}O_{12}$ in ref. 6 by XANES measurements at the Ru-L_{III} absorption edge. This is in agreement with $\delta = 0$ obtained by thermogravimetry for the pure ruthenates $LaCu_3Ru_4O_{12}$ and $NdCu_3Ru_4O_{12}$.[19] The effect of the excess oxygen observed in $Ln_yCu_3Ru_xTi_{4-x}O_{12+\delta}$ on the valences of Cu and Ru is examined in the following.

4.1 Ru-K edge studies

XANES measurements were performed at the Ru-K absorption edge for all three A-site cation series (La, Pr, and Nd), which allows a direct comparison of the Ru-valence properties. The normalized spectra of the Ru-K edge of selected $Ln_yCu_3Ru_xTi_{4-x}O_{12+\delta}$ samples are shown in Fig. 4 in the ESI.† The edge-shape is very similar for all samples showing two distinct peaks which result from the transition from the 1s into the 5p like orbitals. A pre-edge feature caused by the quadrupole allowed transitions into 4d states is not observed, which is in agreement with the highly symmetrical octahedral coordination of the B-site.

At the K-edges the inflection point of the absorption edge (determined as the first maximum in the first derivative) is typically used to calculate the valence.[27–29] In Fig. 4 the obtained edge energies are shown as a function of the nominal ruthenium oxidation state assuming a constant Cu^{2+} valence. The open symbols correspond to the edge energies of the reference materials. The observed valence shift for the references is clearly linear and amounts to ≈ 1.9 eV per oxidation state (similar to ref. 28) as marked by the diagonal solid line according to the linear relation

$$E_{Ru-K}(keV) = 22.1219 + 0.0019\ (\text{nominal Ru valence}). \quad (4)$$

The additionally shown dashed lines indicate an error range of approximately ±0.2 eV. As can easily be seen, the edge energies of the $Ln_yCu_3Ru_xTi_{4-x}O_{12+\delta}$ samples do not vary with the ruthenium content but remain almost constant at a value typical for oxides containing Ru^{4+}. The energy value for $x = 0.5$ of the La series is not shown for graphical reasons, but also amounts to 22.1297 keV, *i.e.* close to Ru^{4+}. It can be concluded that the ruthenium oxidation state is constantly +4 ($4d^4$ configuration) in all samples in agreement with investigations at the Ru-L_{III} edge.[6]

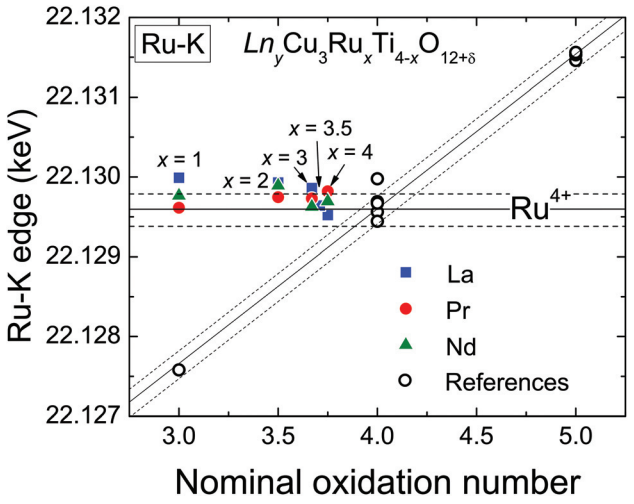

Fig. 4 (color online) Absorption-edge energies in $Ln_yCu_3Ru_xTi_{4-x}O_{12+\delta}$ as derived from the Ru-K XANES spectra analysis as a function of the nominal Ru valence assuming Cu^{2+}. Open circles represent the reference materials.

4.2 Cu-K edge studies

In contrast to the Ru-K edge, the Cu-K spectra depicted in Fig. 5 show a clear dependence on the substitution level. For $La_{2/3}Cu_3Ti_4O_{12}$ (top) a well-pronounced and sharp structure of the absorption edge is visible, which remains almost unchanged up to $x = 2.0$. A small pre-edge feature denoted as P is detectable as well as four distinct peak-like structures denoted A to D. Starting with the spectrum of $LaCu_3Ru_{2.5}Ti_{1.5}O_{12}$ these peaks become broader and the shape of the absorption edge of the pure ruthenate (bottom) becomes visibly smoother.

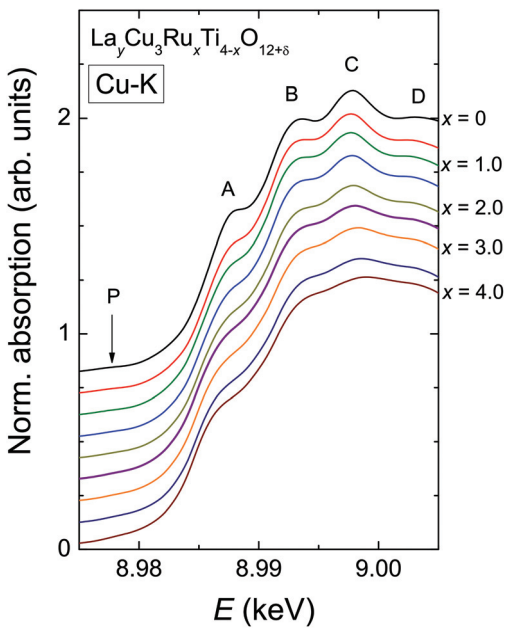

Fig. 5 (color online) Normalized Cu-K edge XANES spectra of $La_yCu_3Ru_x$-$Ti_{4-x}O_{12+\delta}$ for selected substitution levels x in steps of 0.5. The spectra were vertically shifted by 0.1 to increase comparability.

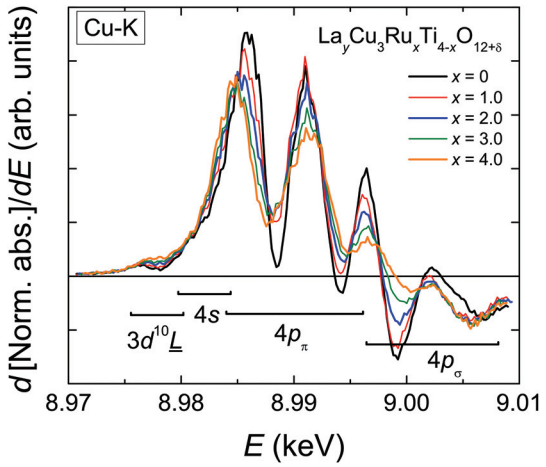

Fig. 6 (color online) First derivative of the normalized Cu-K edge XANES spectra of $La_yCu_3Ru_xTi_{4-x}O_{12+\delta}$ for selected substitution levels x.

The derivatives of the Cu-K edge spectra are shown in Fig. 6. The small pre-edge feature of the excitation in the $3d^{10}\underline{L}$ hole state gradually becomes smaller with increasing x. This indicates a decreasing number of holes due to a reduced average valence. The four distinct peaks A–D correspond to transitions to 4p type orbitals.[29–34] However, in peak A a rather strong contribution of the quadrupole allowed transitions of 4s states to the 4p transitions might be present due to the square-planar coordination of the copper ions. In agreement with the increasing softening of the absorption-edge shape seen in Fig. 6 the peaks broaden and their heights decrease upon increasing Ru substitution.

The edge energies determined from the maxima of the first derivatives of peak A (see Fig. 6) for the complete series $Ln_yCu_3Ru_xTi_{4-x}O_{12+\delta}$ are depicted as a function of the Ru-substitution level in Fig. 7. The edge energies linearly decrease with increasing x from the pure titanates to the pure ruthenates, which is marked by the solid line. $CaCu_3Ti_4O_{12}$ and $SrCu_3Ti_4O_{12}$ were used as Cu^{2+} references (marked by orange stars in Fig. 7). For these compounds, the presence of divalent copper has earlier been confirmed from charge neutrality, specific heat, magnetic susceptibility, and electron-paramagnetic-resonance (EPR) spectroscopy.[35] The edge energies of these two references and the pure titanates $Ln_{2/3}Cu_3Ti_4O_{12}$ (Ln = La, Pr, Nd) are almost equal (±0.2 eV), which proves the presence of Cu^{2+} ions in pure titanates. These XANES results are in agreement with EPR measurements reported in ref. 36.

Absolute values for the copper oxidation states can be obtained using the difference of the absorption edge energies between Cu_2O and CuO as references for Cu^{1+} and Cu^{2+}. This difference amounts to 3.1 eV from our own measurements, which is in good agreement with the average difference of 3.3(2) eV reported in literature.[30,37–39] From the linear fit

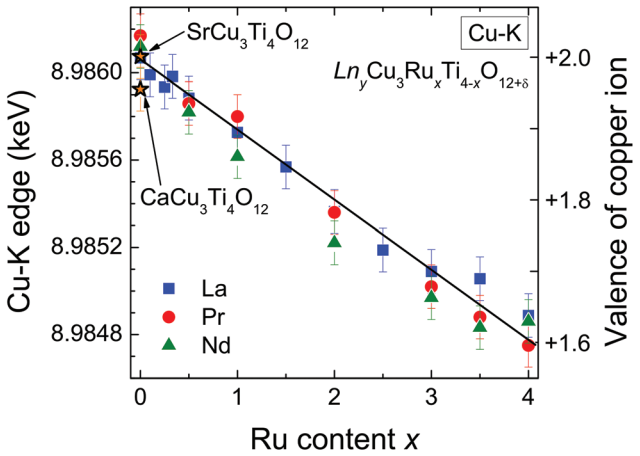

Fig. 7 (color online) Cu-K absorption edge energies of $Ln_yCu_3Ru_xTi_{4-x}O_{12+\delta}$. The solid line marks the linear decrease with increasing Ru content. On the right scale the estimated copper valence determined from the edge shift is marked. For details see text.

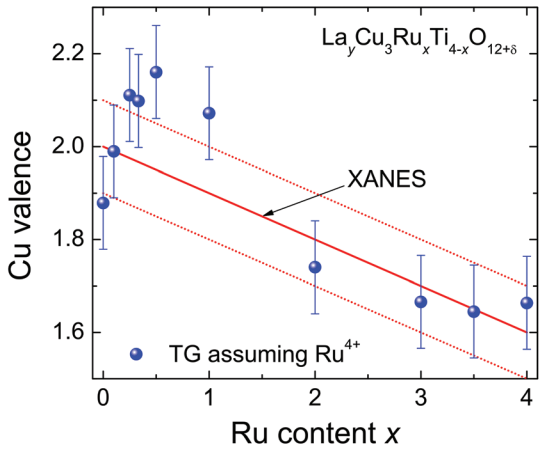

Fig. 8 (color online) Nominal Cu valence of $La_yCu_3Ru_xTi_{4-x}O_{12+\delta}$ determined from XANES (solid line) and TG analysis (symbols) assuming tetravalent Ru.

shown in Fig. 7 a decrease of the edge energy by $\Delta E \approx 1.3$ eV between $x = 0$ and $x = 4$ is obtained. Using this value, a Cu valence of approximately +1.6 for the pure ruthenates can be calculated according to $\Delta E/[E(\mathrm{CuO}) - E(\mathrm{Cu_2O})] = 1.3/3.1 \approx 0.42$. In other words, the nominal copper oxidation state decreases linearly by 0.1 per integer value of x upon substitution as illustrated by the right scales in Fig. 7. The value of +1.6 for $LnCu_3Ru_4O_{12}$ is in good agreement with the calculated valence of +1.67 assuming Ru^{4+} and $\delta = 0$.

The non-integer oxidation state could be a hint for the existence of mono- and divalent Cu ions. However, the absorption-edge spectra do not provide any shoulders or additional steps indicating a coexistence of Cu^{1+} and Cu^{2+} as found *e.g.* for rapidly cooled samples of the closely related system $Cu_{2+x}Ta_4O_{12+\delta}$.[6] This result reveals that all Cu ions possess the same average valence supporting arguments of increasing itinerancy of electrons for increasing Ru content reported for this system.[4,6]

The XANES results for the $Ln_yCu_3Ru_xTi_{4-x}O_{12+\delta}$ series are remarkably different from the results of the valence evolution observed for the perovskite-related Ruddlesden–Popper system $La_{2-x}Sr_xCu_{1-y}Ru_yO_{4-\delta}$ with mixed Ru/Cu-site. These compounds contain divalent copper and provide a change of the Ru valence between +4 and +5 depending on the substitution levels.[22,40,41]

4.3 Comparison of TG and XANES results

The Cu oxidation state obtained by XANES spectroscopy can be compared with the one from the TG weight loss assuming fixed tetravalent Ru. The obtained valence of copper is depicted in Fig. 8. The solid line marks the oxidation state resulting from the energy shift of the Cu-K absorption edge. The TG data and XANES results are generally in good agreement within the estimated experimental uncertainties except for the samples with low Ru substitution levels $x = 0.5$ and $x = 1.0$, which according to the TG results would show a higher valence than expected. This may be explained by a small off-stoichiometric amount of Cu in the samples, which is most likely incorporated on the A-sites due to the sample preparation using a CuO flux. It should be kept in mind that for $\delta = 0$ a constant Cu valence of +1.67 would result for $x \geq 0.1$, a behavior, which is clearly not observed.

5 Conclusions

The combination of TG and XAS investigations provides important information on the mixed valence states of copper and ruthenium containing oxides.[42] It was found that in $Ln_yCu_3Ru_xTi_{4-x}O_{12+\delta}$ (Ln = La, Pr, Nd) considerable amounts of excess oxygen up to $\delta \approx 0.7$ can be incorporated. This finding is in accordance with earlier reports on $Cu_{2+x}Ta_4O_{12+\delta}$.[26]

XANES investigations at the Ru-K edge confirm a constant oxidation state of +4 for ruthenium, independent of the La/Ru/Ti-composition. On the other hand, the oxidation state of copper was found to vary between +2 for the pure titanates $Ln_{2/3}Cu_3Ti_4O_{12}$ and +1.6 for the ruthenates $LnCu_3Ru_4O_{12}$. Lower Cu valences for the Ti-rich compounds are avoided by the excess oxygen content δ. Small deviations between copper oxidation numbers obtained from thermogravimetry and X-ray absorption spectroscopy at low x values may derive from additional Cu ions on the A-site.

Our results are of high importance for the interpretation of the electronic and magnetic properties of the $La_yCu_3Ru_xTi_{4-x}O_{12+\delta}$ samples. The observed metal-to-insulator transition as well as the variation of magnetic properties depending on the ruthenium content are in accordance with constant Ru and changing non-integer Cu valences.[4,5,18] Due to the decreasing Cu oxidation state the itinerancy of the 3d electrons increases with the increasing Ru substitution level until the transition to the metallic heavy-fermion behavior is observed at $x \approx 2.25$.[17]

Even in this heavy-fermion phase a change of the Kondo physics can be observed, which is closely related to the varying electronic properties in the correlated Cu and Ru systems.[18] In contrast, the copper valence in the related $CaCu_3Ru_4O_{12}$ was determined to be +2,[43] which evidences varying electronic correlations driving the heavy-fermion properties in the $ACu_3Ru_4O_{12}$ compounds depending on the element occupying the A-site. This was also reported by Mizumaki *et al.*[44] where an increasing number of O 2p holes and decreasing charge-transfer energy for $LaCu_3Ru_4O_{12}$, $CaCu_3Ru_4O_{12}$, and $NaCu_3Ru_4O_{12}$ were found. Furthermore, in agreement with the changing number of hole states a duality of localized and itinerant character of the Cu 3d electrons was concluded as it is evidenced by this work as well. Also, since the Pr and Nd series provide similar electronic, magnetic, and valence properties like $La_yCu_3Ru_xTi_{4-x}O_{12+\delta}$, analog oxygen stoichiometries and heavy-fermion physics can be assumed and deserves more detailed investigation.

Acknowledgements

The authors gratefully acknowledge HASYLAB (DESY) for allocating beamtime and E. Welter for technical support. This work was supported by the Bavarian graduate school (Resource strategy concepts for sustainable energy systems) of the Institute of Materials Resource Management (MRM) of the University of Augsburg and partly by the DFG within the collaborative research unit TRR 80 (Augsburg, Munich, and Stuttgart).

References

1 A. M. Glazer, *Acta Crystallogr., Sect. B: Struct. Crystallogr. Cryst. Chem.*, 1972, **28**, 3384–3392.
2 P. M. Woodward, *Acta Crystallogr., Sect. B: Struct. Sci.*, 1997, **53**, 32–43.
3 A. N. Vasil'ev and O. S. Volkova, *Low Temp. Phys.*, 2007, **33**, 895–914.
4 A. P. Ramirez, G. Lawes, D. Li and M. A. Subramanian, *Solid State Commun.*, 2004, **131**, 251–255.
5 N. Büttgen, H.-A. K. von Nidda, W. Kraetschmer, A. Günther, S. Widmann, S. Riegg, A. Krimmel and A. Loidl, *J. Low Temp. Phys.*, 2010, **161**, 148–166.
6 S. G. Ebbinghaus, S. Riegg, T. Götzfried and A. Reller, *Eur. Phys. J. Spec. Top.*, 2010, **180**, 91–116.
7 M. A. Subramanian, D. Li, N. Duan, B. A. Reisner and A. W. Sleight, *J. Solid State Chem.*, 2000, **151**, 323–325.
8 M. A. Subramanian and A. W. Sleight, *Solid State Sci.*, 2002, **4**, 347–351.
9 J. Sebald, S. Krohns, P. Lunkenheimer, S. G. Ebbinghaus, S. Riegg, A. Reller and A. Loidl, *Solid State Commun.*, 2010, **150**, 857–860.
10 I. Tsukada, R. Kammuri, T. Kida, S. Yoshii, T. Takeuchi, M. Hagiwara, M. Iwakawa, W. Kobayashi and I. Terasaki, *Phys. Rev. B: Condens. Matter*, 2009, **79**, 054430.
11 S. Kondo, D. C. Johnston, C. A. Swenson, F. Borsa, A. V. Mahajan, L. L. Miller, T. Gu, A. I. Goldman, M. B. Maple, D. A. Gajewski, E. J. Freeman, N. R. Dilley, R. P. Dickey, J. Merrin, K. Kojima, G. M. Luke, Y. J. Uemura, O. Chmaissem and J. D. Jorgensen, *Phys. Rev. Lett.*, 1997, **78**, 3729.
12 A. Krimmel, A. Loidl, M. Klemm, S. Horn and H. Schober, *Phys. Rev. Lett.*, 1999, **82**, 2919.
13 W. Kobayashi, I. Terasaki, J. Takeya, I. Tsukada and Y. Ando, *J. Phys. Soc. Jpn.*, 2004, **73**, 2373.
14 A. Krimmel, A. Günther, W. Kraetschmer, H. Dekinger, N. Büttgen and A. Loidl, *Phys. Rev. B: Condens. Matter*, 2008, **78**, 165126.
15 S. Tanaka, N. Shimazui, H. Takatsu, S. Yonezawa and Y. Maeno, *J. Phys. Soc. Jpn.*, 2009, **78**, 024706.
16 A. Krimmel, A. Günther, W. Kraetschmer, H. Dekinger, N. Büttgen, V. Eyert, A. Loidl, D. Sheptyakow, E.-W. Scheidt and W. Scherer, *Phys. Rev. B: Condens. Matter*, 2009, **80**, 121101.
17 B. Schmidt, H.-A. K. von Nidda, S. Riegg, S. G. Ebbinghaus, A. Reller and A. Loidl, *Magn. Reson. Solids*, 2014, **16**, 14210.
18 S. Riegg, S. Widmann, A. Günther, S. Wehrmeister, S. Sterz, W. Kraetschmer, S. G. Ebbinghaus, A. Reller, N. Büttgen, H.-A. K. von Nidda and A. Loidl, *Eur. Phys. J. Spec. Top.*, 2015, accepted.
19 S. G. Ebbinghaus, A. Weidenkaff and R. J. Cava, *J. Solid State Chem.*, 2002, **167**, 126–136.
20 J. Rodriguez-Carvajal, *Physica B*, 1993, **192**, 55–69.
21 J. A. Bearden and A. F. Burr, *Rev. Mod. Phys.*, 1967, **39**, 125–142.
22 S. G. Ebbinghaus, Z. Hu and A. Reller, *J. Solid State Chem.*, 2001, **156**, 194–202.
23 R. D. Shannon, *Acta Crystallogr., Sect. A: Cryst. Phys., Diffr., Theor. Gen. Cryst.*, 1976, **32**, 751–767.
24 J. Muller, A. Haouzi, C. Laviron, M. Labeau and J. C. Joubert, *Mater. Res. Bull.*, 1986, **21**, 1131–1136.
25 H. R. Oswald, S. Felder-Cassagrande and A. Reller, *Solid State Ionics*, 1993, **63–65**, 565–569.
26 S. G. Ebbinghaus, *Prog. Solid State Chem.*, 2007, **35**, 421–431.
27 *X-Ray Absorption*, ed. D. C. Koningsberger and S. Prins, John Wiley and Sons, New York, 1988.
28 J.-H. Choy, J.-Y. Kim, S.-H. Hwang, S.-J. Kim and G. Demazeau, *Int. J. Inorg. Mater.*, 2000, **2**, 61–70.
29 C. L. Chen, S. M. Rao, K. J. Wang, F. C. Hsu, Y. C. Lee, C. L. Dong, T. S. Chan, J. F. Lee, M. C. Ling, H. L. Liu and M. K. Wu, *New J. Phys.*, 2009, **11**, 073024.
30 E. E. Alp, G. K. Shenoy, D. G. Hinks, D. W. C. II, L. Soderholm, H. B. Schuttler, J. Guo, D. E. Ellis, P. A. Montano and M. Ramanathan, *Phys. Rev. B: Condens. Matter*, 1987, **35**, 7199.
31 N. Kosugi, H. Kondoh, H. Tajima and H. Kuroda, *Chem. Phys.*, 1989, **135**, 149–160.
32 S. K. Pandey, A. R. Chetal and P. R. Sarode, *Physica B*, 1991, **172**, 324–328.

33 J.-H. Choy, D.-K. Kim, S.-H. Hwang and G. Demazeau, *Phys. Rev. B: Condens. Matter*, 1994, **50**, 16631.
34 Z. Wu, M. Benfatto and C. R. Natoli, *Phys. Rev. B: Condens. Matter*, 1996, **54**, 13409.
35 M. A. Pires, C. Israel, W. Iwamoto, R. R. Urbano, O. Agüero, I. Torriani, C. Rettori, P. G. Pagliuso, L. Walmsley, Z. Le, J. L. Cohn and S. B. Oseroff, *Phys. Rev. B: Condens. Matter*, 2006, **73**, 224404.
36 A. Dittl, S. Krohns, J. Sebald, F. Schrettle, M. Hemmida, H.-A. K. von Nidda, S. Riegg, A. Reller, S. G. Ebbinghaus and A. Loidl, *Eur. Phys. J. B*, 2011, **79**, 391–400.
37 Y. Y. Hsu, B. N. Lin, J. F. Lee, L. Y. Jang and H. C. Ku, *J. Low Temp. Phys.*, 2003, **131**, 343–347.
38 X. Wang, J. A. Rodriguez, J. C. Hanson, D. Gamarra, A. Martinez-Arias and M. Fernandez-Garcia, *J. Phys. Chem. B*, 2005, **109**, 19595–19603.
39 S. Bijani, M. Gabas, G. Subias, J. Garcia, L. Sanchez, J. Morales, L. Martinez and J.-R. Ramos-Barrado, *J. Mater. Chem.*, 2011, **21**, 5368–5377.
40 S. Ebbinghaus, M. Fröba and A. Reller, *J. Phys. Chem. B*, 1997, **101**, 9909–9915.
41 S. Ebbinghaus and A. Reller, *Solid State Ionics*, 1997, **101–103**, 1369–1377.
42 S. Riegg, T. Müller and S. G. Ebbinghaus, *Solid State Sci.*, 2013, **20**, 97–102.
43 N. Hollmann, Z. Hu, A. Maignan, A. Günther, L.-Y. Jang, A. Tanaka, H.-J. Lin, C. T. Chen, P. Thalmeier and L. H. Tjeng, *Phys. Rev. B: Condens. Matter*, 2013, **87**, 155122.
44 M. Mizumaki, T. Mizokawa, A. Agui, S. Tanaka, H. Takatsu, S. Yonezawa and Y. Maeno, *J. Phys. Soc. Jpn.*, 2013, **82**, 024709.